FINITE ELEMENT MODEL FOR PREDICTING THE SHEAR BEHAVIOR OF FRP-STRENGTHENED RC MEMBERS

Mehdi Zomorodian, Ph.D. [1], Abdeldjelil Belarbi[2*], Ph.D., P.E., Ashraf Ayoub, Ph.D., P.E.[3]

[1]Structural Engineer, Matrix Structural Engineers, Houston, USA. E-mail: mzomorodian@matrixstructural.com

[2*]Hugh Roy and Lillie Cranz Cullen Distinguished Professor, Department of Civil and Environmental Engineering, University of Houston, Houston, USA. E-mail: belarbi@uh.edu

[3]Professor, City, University of London. E-mail: Ashraf.Ayoub.1@city.ac.uk

ABSTRACT

The shear behavior of FRP strengthened reinforced concrete (FRP strengthened RC) membrane elements can be predicted by developing logical models that satisfy the principles of mechanics of materials namely stress equilibrium, strain compatibility, and constitutive relationships of concrete, steel bars and, FRP reinforcements. The Softened Membrane Model (SMM), which was developed for predicting the shear behavior of reinforced concrete (RC) membrane elements, is extended to FRP strengthened RC members subjected to shear. This new analytical model, referred to as the Softened Membrane Model for FRP strengthened RC members (SMM-FRP), considers new constitutive laws for each material component of the member. Similar to the case of the SMM model for RC, this new SMM-FRP model can predict the entire stress-strain curve, including pre- and post-cracking, and the ascending and descending branches. The SMM-FRP is implemented into an OpenSees-based finite element program for a membrane 2-D element that will allow structural engineers to predict the monotonic responses of FRP strengthened RC members subjected to shear. The developed program is validated in this paper by the prediction of the monotonic responses of 10 FRP strengthened RC panels subjected to pure shear stresses. The good agreement between the experimental and analytical results

confirms the validity of the analytical model in predicting the shear behavior of RC members strengthened with FRP sheets.

1. INTRODUCTION

To predict the increase in shear capacity due to FRP strengthening, several analytical models have been proposed. However, when these models are used to predict other researcher's experimental results, they show inconsistencies and large scatters in predictions. A high level of complexity exists in the shear behavior, but lack of accurate material models for FRP strengthened RC members results in these discrepancies. These models are based on test results of simply supported beam specimens with various shear spans to depth ratios. In such tests no region of the specimen is subjected to uniform stress conditions, Therefore, the results of such tests cannot predict the true pure shear behavior due to non-uniformity of stresses, the presence of flexural, and other non-shear related effects that cannot be filtered out. Therefore, precise shear design theories cannot be developed. The constitutive behavior of RC and FRP were defined independently in these models. The rational behavior, however, should account for the high level of interactions between the concrete, steel and FRP. Also, different parameters that might influence this phenomenon such as the softening of concrete under biaxial stress field, and the representative constitutive laws of concrete, steel and FRP in tension should be considered. Furthermore, the constitutive laws of materials used in conjunction with these models are based on previously developed relations for conventional reinforced concrete elements, which may not be valid for strengthened elements. Before understanding the behavior of FRP strengthened RC members in complex

loading conditions involving shear, the behavior in pure shear conditions must be first understood.

In current design guidelines, the shear capacity of the FRP-strengthened RC members is calculated as a superposition of the shear contribution of concrete, steel, and FRP which were derived independently. However, a high level of interaction exists between these components and different parameters that might influence this interaction need to be taken into account (Bousselham and Chaallal, 2008; Chen et al., 2010).

The presence of the FRP sheets typically alters the crack pattern which will affect the main characteristics of the concrete material (Zomorodian et al., 2016). Specifically, the governing parameters of the softened membrane model (Hsu and Zhu, 2002) needs close investigation. These includes the softening behavior of concrete under biaxial loading, the smeared stress-strain behavior of the constituents of strengthened member including concrete and reinforcing steel, and the post-cracking Poisson ratio, which will be fundamentally different than their corresponding values for un-strengthened specimens. Consequently, different failure modes are observed, which affects the shear strength of the member. The issue is further complex due to the presence of several additional parameters that might influence the behavior; such as the properties of the FRP material, the angle of fiber axis, the interfacial characteristics of fiber-resin and FRP-concrete, the presence of mechanical anchors, and the use of FRP strips as opposed to continuous sheets. Such additional parameters, arising from the strengthening system, further

modifies the observed failure mode, crack pattern, and also influences the constitutive behavior of reinforced concrete.

An efficient method to evaluate the overall shear response of a member, known as the element-based approach, is to identify the characteristic behavior and the contribution of each element and material constituting the structure (Belarbi, 1991; Hsu et al., 1995). As shown in Fig. 1, an element subjected to shear stresses is separated from a girder strengthened externally by FRP sheets; by taking into account the inherent characteristics and material laws of the constituents the behavior of that specific element can be predicted. This will ultimately lead to understanding the global shear response of the girder. To define the shear behavior of the element a set of equilibrium equations, compatibility conditions, and materials laws for steel and FRP reinforcements in the longitudinal *l* and transverse *t* directions as well as the concrete in tension and compression in the principal 1 and 2 directions, respectively are required.

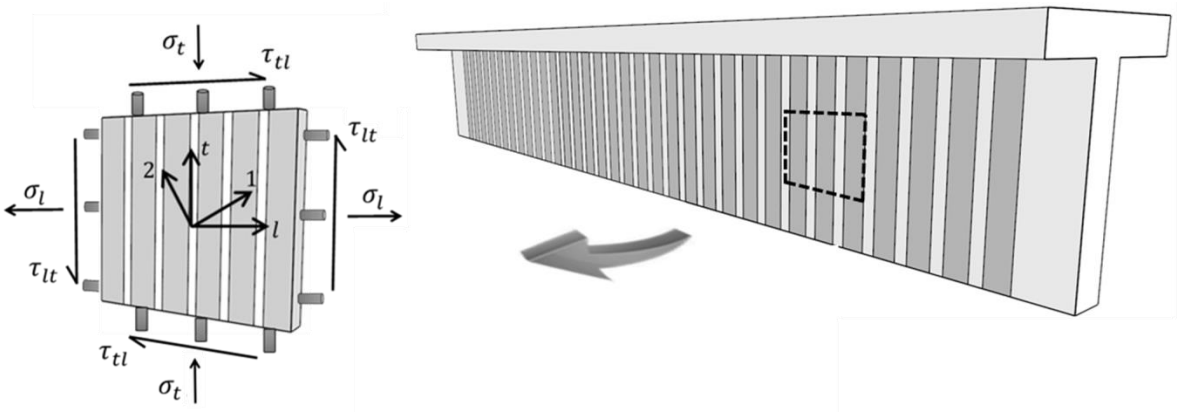

Fig. Error! No text of specified style in document.**.** Beam Shear Element with In-Plane Stresses (adopted from Yang et al, 2014)

At the University of Houston, a Universal Panel Tester was constructed which is capable of

testing full-size elements (1.398 m × 1.398 m × 0.178 m) as shown in Fig. 2. From the experimental behavior of representative elements tested in the Panel Tester, new analytical models can be established. The response of a structure can be predicted by integrating these analytical models into finite element programs. Following the element-based approach, during the past decade over 90 panel elements were subjected to monotonic loading to study the shear behavior of reinforced concrete elements. As a result, three analytical models were developed, namely: the rotating-angle softened truss model (Belarbi and Hsu, 1994, 1995; Pang and Hsu, 1995), the fixed-angle softened truss model (Pang and Hsu, 1996; Hsu and Zhang 1997), and the softened membrane model (SMM) (Hsu and Zhu, 2002).

To study the shear behavior of FRP-strengthened RC elements, a total of 10 panel elements were subjected to pure shear loading. The experimental behavior of such elements will be presented in a companion paper. A new softened membrane model for FRP-strengthened RC members (SMM-FRP) was developed from the observed behavior. The SMM-FRP is an extension of the SMM for RC members.

To expand the use of the SMM to predict the behavior of the FRP-strengthened RC members subjected to pure shear, new constitutive laws for each material component of the member, namely, concrete, embedded steel, and externally bonded FRP, should be established. The material laws of concrete in SMM-FRP includes: concrete in tension, concrete in compression, and concrete in shear. The material laws of reinforcements in SMM-FRP includes: steel in tension and FRP in tension.

This paper summarizes the new analytical model by presenting the equilibrium and compatibility equations , the constitutive material model, the concept of biaxial strains versus uniaxial strains,

the solution algorithm. To further validate the model the comparison of the SMM-FRP predictions with the test results of 10 panels are presented. . Furthermore, a nonlinear reinforced concrete finite element program is developed by implementing the SMM-FRP into the finite element framework OpenSees (McKenna and Fenves 2001). The finite element program is validated through comparison with experimental results of panel specimens.

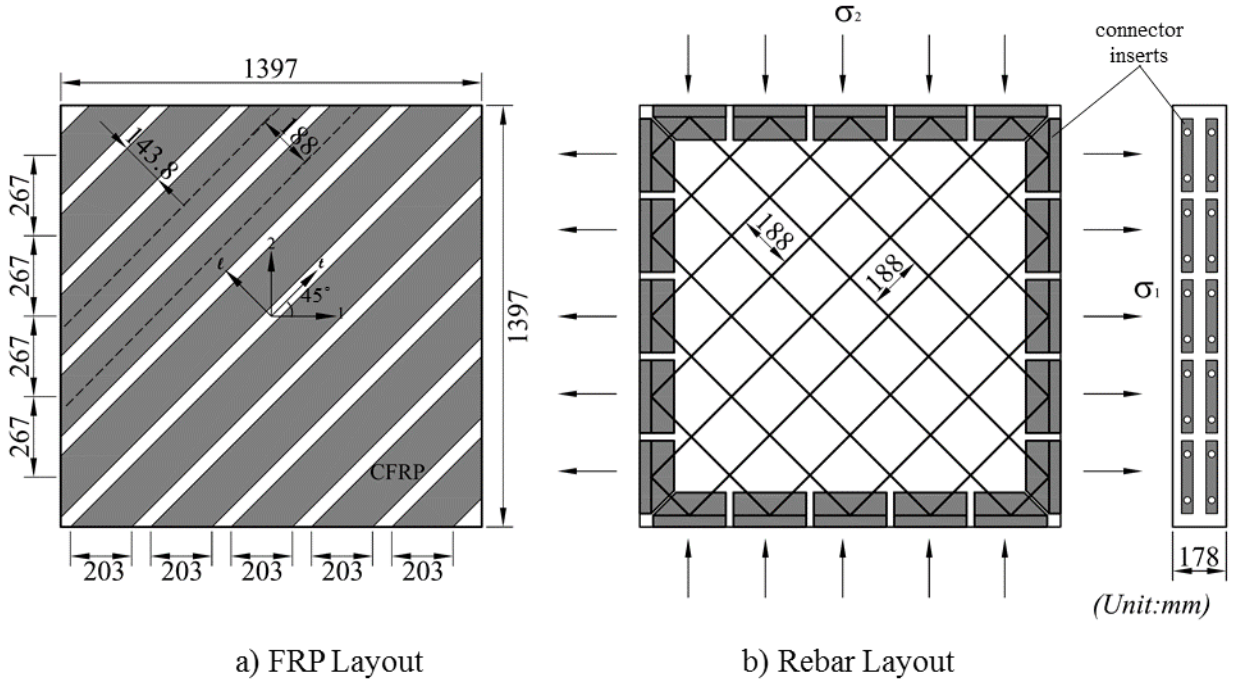

Fig. 2. Dimensions of Test Panels

2. Softened Membrane Model for FRP-Strengthened RC Elements

The SMM-FRP satisfies Navier's three principles of mechanics of materials, namely (1) the equilibrium equations, (2) the compatibility equations, and (3) the constitutive laws for concrete, steel, and FRP. Fig. 3a shows an FRP-strengthened RC element subjected to in-plane membrane stresses. This element is based on superposition of several components, namely concrete element (Fig. 3b), steel grid element (Fig. 3c) and FRP strip element (Fig. 3d). Similar to the SMM, two

coordinate systems are used in the SMM-FRP, as shown in Fig. 3e. The l-*t* coordinate system represents the directions of longitudinal and transversal reinforcements. The s 1-2 coordinate system represents the directions of the principal compressive stress (2-axis) and tensile stress (1-axis). In SMM-FRP, the cracks are assumed to occur along the principal 2-axis. After cracking, the concrete element is divided into several struts that carry compression stress, σ_2, in 2-axis, also the tension stress, σ_1, in 1-axis (see Fig. 3e-f).

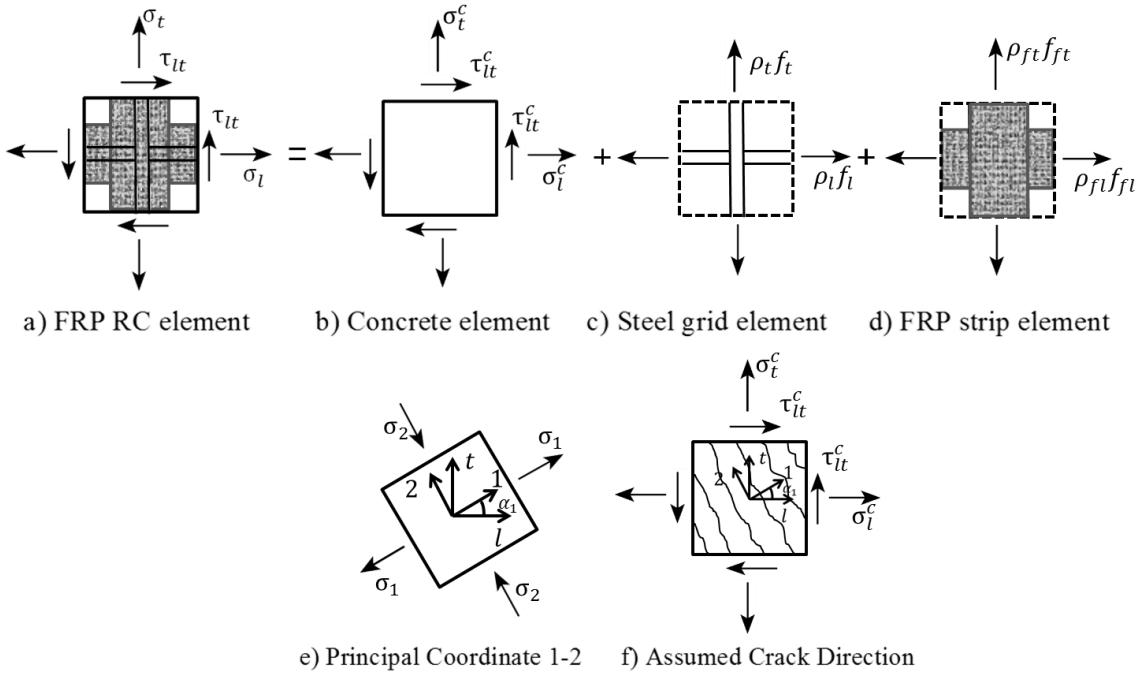

Fig. 3. Stress Diagram for FRP Strengthened RC Element Subjected to In-Plane Stresses (adopted from Hsu and Mo, 2010)

To predict the behavior of the FRP-RC element shown in Fig. 3a, the stress-strain relationships of concrete, steel, and FRP are required in terms of the principal tensile direction (1-axis) and the principal compressive direction (2-axis). In the steel element, since no dowel actions are considered, only constitutive laws of steel in tension (in *l* and *t* directions) are required. Similar to the steel reinforcement, the constitutive laws of FRP in tension (in *l* and *t* direction) are

needed. An FRP-RC element subjected to shear is in the state of biaxial stresses and strains; therefore, in order to use the uniaxial material laws in the SMM-FRP model, the biaxial strains have to be transferred into uniaxial strain by involving the Poisson ratio. Once the biaxial principal strains ε_1 and ε_2 along the direction of applied tensile and compressive loads are evaluated, the Poisson ratios of cracked concrete are required to derive the equivalent uniaxial strains in 1 and 2 directions.

2.1. Equilibrium and Compatibility Equations

The three equilibrium equations (stress transformation equations), which relate the applied stresses (σ_l, σ_t, and τ_{tl}) to the internal stresses of concrete (σ_2^c, σ_1^c, and τ_{12}^c), steel rebar (f_l and f_t), and FRP sheets (f_{ft} and f_{fl}) in a membrane element, are expressed as

$$\sigma_l = \sigma_1^c \cos^2\alpha_1 + \sigma_2^c \sin^2\alpha_1 - \tau_{12}^c 2\sin\alpha_1\cos\alpha_1 + \rho_l f_l + \rho_{fl} f_{fl} \quad (1)$$

$$\sigma_t = \sigma_1^c \sin^2\alpha_1 + \sigma_2^c \cos^2\alpha_1 + \tau_{12}^c 2\sin\alpha_1\cos\alpha_1 + \rho_t f_t + \rho_{ft} f_{ft} \quad (2)$$

$$\tau_{lt} = \left(\sigma_1^c - \sigma_2^c\right)\sin\alpha_1\cos\alpha_1 + \tau_{12}^c\left(\cos^2\alpha_1 - \sin^2\alpha_1\right). \quad (3)$$

In Eqns. (1) and (2), in addition to the contributions of concrete and steel, two additional terms $\rho_{fl} f_{fl}$ and $\rho_{ft} f_{ft}$ are incorporated into the original equilibrium equations of SMM to include the tensile contributions of FRP in the *l* and *t* directions.

The three compatibility equations for FRP-strengthened RC elements are the same as the equations of RC elements. The compatibility equations which represent the transformation between the biaxial strains (ε_l, ε_t, and γ_{lt}) in the *l*-*t* coordinate system along the direction of reinforcements and the biaxial strains (ε_1, ε_2, and γ_{12})

in the 1-2 coordinate system along the direction of applied principle stress are given as follow:

$$\varepsilon_l = \varepsilon_1 \cos^2 \alpha_1 + \varepsilon_2 \sin^2 \alpha_1 - \frac{\gamma_{12}}{2} 2 \sin \alpha_1 \cos \alpha_1 \quad (4)$$

$$\varepsilon_t = \varepsilon_1 \sin^2 \alpha_1 + \varepsilon_2 \cos^2 \alpha_1 + \frac{\gamma_{12}}{2} 2 \sin \alpha_1 \cos \alpha_1 \quad (5)$$

$$\frac{\gamma_{lt}}{2} = (\varepsilon_1 - \varepsilon_2) \sin \alpha_1 \cos \alpha_1 + \frac{\gamma_{12}}{2} (\cos^2 \alpha_1 - \sin^2 \alpha_1) \quad (6)$$

The compatibility conditions, defined by Eqns. (4-6) contain six variables, namely, ε_l, ε_t, γ_{lt}, ε_1, ε_2, and γ_{12}. To solve the three equilibrium and the three compatibility equations,the stress-strain relationships of concrete, steel rebars, and FRP sheets are required.

2.2. Biaxial Strains vs. Uniaxial Strains

To correlate stresses in the equilibrium formulations to strains in the compatibility formulations, the stress-strain relationships of concrete, stee and FRP reinforcements are required. The shear element is in the state of biaxial stress, therefore, the set of strains used in the compatibility equations given in Eq. (4) through Eq. (6) are expressed as biaxial strains. The constitutive laws between stresses and biaxial strains are related to uniaxial strains through the Poisson ratios of cracked concrete. The Poisson effect has to be considered in the softened membrane model since all the material laws were developed based on uniaxial tests (Hsu and Zhu, 2002). In order to use uniaxial material laws in the SMM-FRP model, the biaxial strains in the shear element are transferred into uniaxial strains by using

the Poisson ratio. The relationships between the uniaxial strains ($\bar{\varepsilon}_1$, $\bar{\varepsilon}_2$, $\bar{\varepsilon}_l$ and $\bar{\varepsilon}_t$) and the biaxial strains (ε_1, ε_2, ε_l, and ε_t) are given by Zhu (2000) as:

$$\bar{\varepsilon}_1 = \frac{1}{1-\upsilon_{12}\upsilon_{21}}\varepsilon_1 + \frac{\upsilon_{12}}{1-\upsilon_{12}\upsilon_{21}}\varepsilon_2 \tag{7}$$

$$\bar{\varepsilon}_2 = \frac{\upsilon_{21}}{1-\upsilon_{12}\upsilon_{21}}\varepsilon_1 + \frac{1}{1-\upsilon_{12}\upsilon_{21}}\varepsilon_2 \tag{8}$$

$$\bar{\varepsilon}_l = \bar{\varepsilon}_1 \cos^2\alpha_1 + \bar{\varepsilon}_2 \sin^2\alpha_1 - \frac{\gamma_{12}}{2} 2\sin\alpha_1 \cos\alpha_1$$

(9)

$$\bar{\varepsilon}_t = \bar{\varepsilon}_1 \sin^2\alpha_1 + \bar{\varepsilon}_2 \cos^2\alpha_1 + \frac{\gamma_{12}}{2} 2\sin\alpha_1 \cos\alpha_1 . \tag{10}$$

Due to the additional bond action created by the externally bonded FRP sheets, the post cracking Poisson ratios (Hsu/Zhu ratios) are different in case of FRP-strengthened RC members. In previous research conducted by Yang et al. (2015), the Hsu/Zhu ratio was found to be affected mainly by the post-yielding stiffness in the tensile direction. The ratio $\rho_f E_f$ was chosen as the parameter to describe the FRP contribution to the post-yielding stiffness. The following equations were proposed for calculating the Hsu/Zhu ratios ν_{12} and ν_{21} in FRP-strengthened RC members:

$$\nu_{12} = 0.2 + k\varepsilon_{sf} \qquad \text{when } \varepsilon_{sf} \le \varepsilon_y \tag{11a}$$

$$\nu_{12} = 1.9 - 0.00058\rho_f E_f \qquad \text{when } \varepsilon_{sf} > \varepsilon_y \tag{11b}$$

$$\text{where } k = \frac{1.7 - 0.00058\rho_f E_f}{\varepsilon_y} \tag{12}$$

$$\nu_{21} = \begin{cases} 0.2 & \text{Before cracking} \\ 0 & \text{After cracking} \end{cases} \tag{13}$$

where ε_{sf} is the average tensile strain along the reinforcements in l and t directions, whichever yields first.

2.3. Constitutive Relationships of Concrete

In order to use the SMM to predict the behavior of the FRP-strengthened RC members subjected to pure shear, new constitutive laws for each material component of the member have to be established. The material laws of concrete in SMM-FRP includes: concrete in tension, concrete in compression, and concrete in shear. These materials laws were modified based on the tests results presented in this research and tests conducted by Yang et el. (2015, 2017).

The ascending and descending branches of concrete in compression are given by Eqns. (14a) and (14b).The stress-strain relationship of concrete in compression, shown in Fig. 4, is given as:

$$\text{(Stage C1): } \sigma_2^c = \zeta_{FRP} f_c' \left[2\left(\frac{\bar{\varepsilon}_2}{\zeta_{FRP}\varepsilon_0} \right) - \left(\frac{\bar{\varepsilon}_2}{\zeta_{FRP}\varepsilon_0} \right)^2 \right], \text{ when } \frac{\bar{\varepsilon}_2}{\zeta_{FRP}\varepsilon_0} \le 1 \text{ and} \tag{14a}$$

$$\text{(Stage C2): } \sigma_2^c = \zeta_{FRP} f_c' \left[1 - \left(\frac{\left(\bar{\varepsilon}_2 / \zeta_{FRP}\varepsilon_0 \right) - 1}{\left(4/\zeta_{FRP} \right) - 1} \right)^2 \right], \text{ when } \frac{\bar{\varepsilon}_2}{\zeta_{FRP}\varepsilon_0} > 1, \tag{14b}$$

where, ζ_{FRP} is the softening coefficient expressed as

$$\zeta_{FRP} = f(f_c')f(\bar{\varepsilon}_1)f_{FRP}(\beta)f(FRP) \tag{15}$$

where,

$$f(f_c') = \frac{5.8}{\sqrt{f_c'}} \le 0.9 \qquad (f_c' \text{ in MPa}) \tag{16}$$

$$f(\bar{\varepsilon}_1)=\frac{1}{\sqrt{1+400\bar{\varepsilon}_1}}, \tag{17}$$

$$f_{FRP}(\beta)=1-\frac{|\beta|}{16^o}, \tag{18}$$

$$f(FRP)=1+0.0076\sqrt{\rho_f E_f} \quad \text{(in MPa).} \tag{19}$$

A regression analysis of the FRP strengthened RC panels was performed to develop the new function of the deviation angle, β, in the softening coefficient of FRP strengthened RC members (Zomorodian, 2015). The ascending and descending branch of concrete in tension is given by Eqns. (20a) and (20b). The stress-strain relationship of concrete in tension, shown in Fig. 4, is given as (Yang et al., 2015):

$$\text{(Stage T1): } \sigma_1^c = E_c\bar{\varepsilon}_1 \qquad \text{when } \bar{\varepsilon}_1 \le \varepsilon_{cr} \text{ and} \tag{20a}$$

$$\text{(Stage T2): } \sigma_1^c = f_{cr}\left(\frac{\varepsilon_{cr}}{\bar{\varepsilon}_1}\right)^c \qquad \text{when } \bar{\varepsilon}_1 > \varepsilon_{cr}\text{, where} \tag{20b}$$

$$c = k_w k_{f/s}\text{, and} \tag{21}$$

$$K_w = 1 \text{ (Fully wrap or U-wrap with anchors),} \tag{22}$$

$$K_w = 1.6 \text{ (Side bond or U-wrap),} \tag{23}$$

$$K_f = 0.25\left(\frac{\rho_f E_f}{\rho_s E_s}\right)+0.15\,. \tag{24}$$

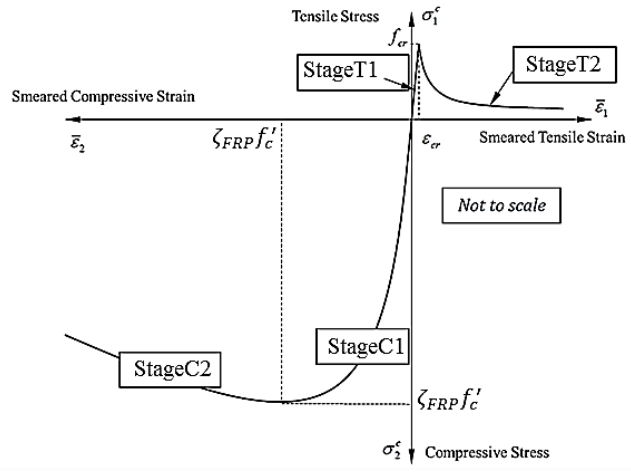

Fig. 4. Constitutive Relationships of Concrete

By using the smeared crack theory, the cracked reinforced concrete strengthened FRP member can be considered as a homogeneous and isotropic material and therefore assuming that the directions of principle stresses and strains coincide, the relationship between the shear stress and strain of cracked concrete in the pricnciple 1-2 coordinate system is derived from equilibrium and compatibility equations. The equation relating concrete shear stress, τ_{12}^{c}, and the concrete shear strain, γ_{12}^{c}, in the 1-2 coordinate system is given as (Zhu et al., 2001):

$$\tau_{12}^{c} = \frac{\left(\sigma_1^{c} - \sigma_2^{c}\right)}{2\left(\varepsilon_1 - \varepsilon_2\right)}\gamma_{12} \tag{25}$$

where, σ_1^{c} and σ_2^{c} are calculated from Eq. (20) and Eq. (14), respectively; ε_1 and ε_2 are biaxial strains in the 1 and 2 directions, respectively.

2.4. Constitutive Relationships of Reinforcements

Two reinforcements are used in FRP-strengthened RC members, namely, steel rebars and externally bonded FRP sheets. In SMM-FRP, the smeared tensile stress-strain relationships of steel reinforcement embedded in concrete are similar to SMM. A bilinear expression was proposed by Belarbi and Hsu (1994) to predict the tensile behavior of steel in RC element. The apparent yielding stress f_y' was proposed to describe the reduction of yielding stress. The equations are:

(Stage 1): $f_s = E_s\bar{\varepsilon}_s \qquad \bar{\varepsilon}_s < \varepsilon_y^{'},$ (26a)

(Stage 2): $f_s = \left(0.91 - 2B\right)f_y + \left(0.02 + 0.25B\right)E_s\bar{\varepsilon}_s \qquad \bar{\varepsilon}_s \geq \varepsilon_y^{'}$ (26b)

(Stage 3): $f_s = f_p - E_s\left(\bar{\varepsilon}_p - \bar{\varepsilon}_s\right)$ $\bar{\varepsilon}_s < \varepsilon_p$ (26c)

where,

$$\varepsilon_y^{'} = f_y'/E_s \qquad f_y' = (0.93 - 2B) f_y \tag{27}$$

$$B = \frac{1}{\rho_{se}}\left(\frac{f_{cr}}{f_y}\right)^{1.5} \tag{28}$$

$$f_{cr} = 3.75\sqrt{f_c'(psi)}\text{, and } \rho_{se} \geq 0.15\% \tag{29}$$

$$\rho_{se} = \rho_s + n_{f/s}\rho_f\text{, where } n_{f/s} = \frac{E_f}{E_s} \tag{30}$$

In the above equations, "s" in the subscript of symbols are replaced by *l* and *t* for longitudinal and transversal steel, respectively.

The smeared stress-strain relationship of FRP sheets in the *l*-*t* coordinate system is expressed as:

$$f_{fs} = E_{fs}\bar{\varepsilon}_{fs} \qquad \bar{\varepsilon}_{fs} < \varepsilon_{fu} \text{ and} \tag{31a}$$

$$f_{fs} = 0 \qquad \bar{\varepsilon}_{fs} \geq \varepsilon_{fu}, \tag{31b}$$

where E_{fs} is the Young's Modulus of Elasticity of the composite, $\bar{\varepsilon}_f$ is the average uniaxial strain of FRP along the fiber direction, and ε_{fu} is the ultimate strain of FRP before it ruptures. In the above equations, *l* replaces s in the subscript of symbols for the longitudinal FRP, and *t* replaces s for the transversal FRP.

3. SOLUTION ALGORITHM

The solution procedure for the SMM-FRP is provided in Fig. 5. There are a total of 22 variables (ε_1, ε_2, γ_{12}, ε_l, ε_t, γ_{lt}, $\bar{\varepsilon}_1$, $\bar{\varepsilon}_2$, $\bar{\varepsilon}_l$, $\bar{\varepsilon}_t$, ν_{21}, ν_{12}, σ_1^c, σ_2^c, τ_{12}^c, σ_l, σ_t, τ_{lt}, f_l, f_t, f_{fl}, and f_{ft}). In pure shear cases, σ_l and σ_t are equal to zero. When a value of ε_2 is selected, the remaining 19 unknown variables can be solved by the 19 independent

equations (6 equations for equilibrium and compatibility, 3 for constitutive laws of concrete, 2 for constitutive laws of steel in *l* and *t* directions, 2 for constitutive laws of FRP in *l* and *t* directions, 4 for relationships relating the strains under uniaxial loading and strains under biaxial loading, and 2 for Hsu/Zhu ratios). The following equations are derived from the equilibrium equations, Eq. (32) and Eq. (33), to make the solution procedure more efficient:

$$\rho_l f_l + \rho_{fl} f_{fl} + \rho_t f_t + \rho_{ft} f_{ft} = (\sigma_l + \sigma_t) - (\sigma_1^c + \sigma_2^c) \tag{32}$$

$$\rho_l f_l + \rho_{fl} f_{fl} - \rho_t f_t - \rho_{ft} f_{ft} = (\sigma_l - \sigma_t) - (\sigma_1^c - \sigma_2^c)\cos 2\alpha_1 + 2\tau_{12}^c \sin 2\alpha_1 \tag{33}$$

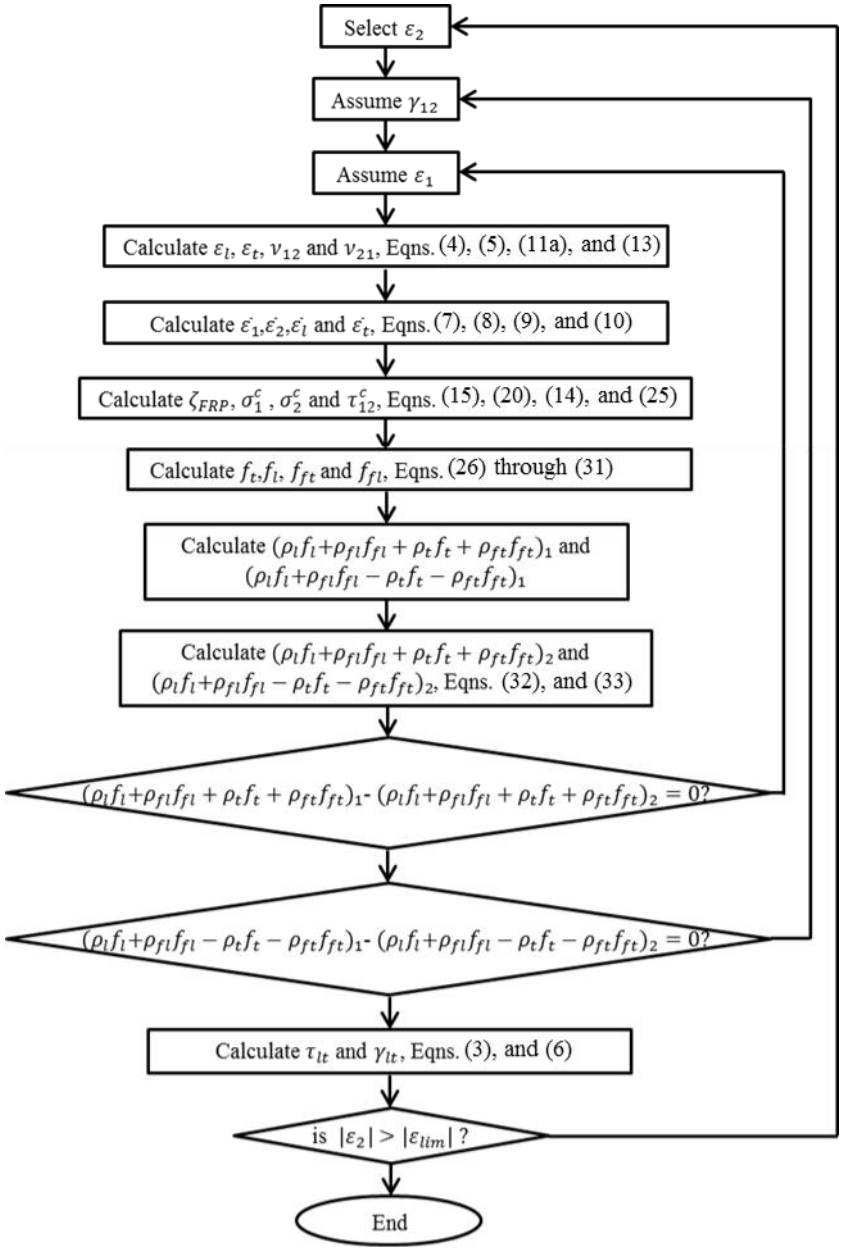

Fig. 5. Flow Chart of Solution Procedure for SMM-FRP

4. Case study of SMM-FRP Calculation Procedure

To illustrate the calculation procedure of SMM-FRP, panel P4-040-FW is taken as an example. Before calculations, the input data of the specimen are presented in Table 1, which includes the concrete compressive strength, $\boldsymbol{f_c'}$, the compressive crushing strain, $\boldsymbol{\varepsilon_0}$, the concrete cracking strain, $\boldsymbol{\varepsilon_{cr}}$, the bare steel bar yielding strength in transversal and longitudinal directions, $\boldsymbol{f_{ty}}$, and

f_{ly}, respectively, the steel ratios ρ_t and ρ_l in transversal and longitudinal direction, respectively, the steel elastic modulus E_s, the FRP reinforcement ratio ρ_f, and FRP elastic modulus E_f.

Table 1 Material Properties for Panel P4-040-FW

f'_c (MPa)	ε_0 (mm/mm)	ε_{cr} (mm/mm)	f_{ly} (MPa)	f_{ty} (MPa)	ρ_l	ρ_t	ρ_f	E_s (MPa)	E_f (MPa)
52	0.002	0.00008	462	462	0.00772	0.00772	0.00876	190000	72000

A computer program is written in MATLAB software according to the solution procedure in Fig. 5. Table 2 gives the calculated results

Table 2 Calculation Results of Panel

Variables	Equation	Calculated Values				
		Crack	First Yield	Second Yield	Peak Point	Descending
ε_2 selected	-	-7.0E-5	-0.00016	-0.000176	-0.000415	-0.003000
ε_1 last assumed	-	0.0001	0.004377	0.005298	0.015028	0.022312
τ_{12}^c last assumed	-	1.76E-7	0.000380	-0.000753	-0.004122	-0.005470
ε_l	(4)	1.4916E-5	0.0022	0.002938	0.009367	0.012391
ε_t	(5)	1.5092E-5	0.0019	0.002184	0.005245	0.012391
ν_{12}	(11)	0.2082	1.536688	1.536688	1.536688	1.536688
$\bar{\varepsilon}_1$	(7)	8.9137E-5	0.004131	0.005028	0.0143907	0.017702
$\bar{\varepsilon}_2$	(8)	-5.2172E-5	-0.00016	-0.000176	-0.000415	-0.00300
$\bar{\varepsilon}_l$	(9)	1.8394E-5	0.00217	0.002803	0.009049	0.010086
$\bar{\varepsilon}_t$	(10)	1.8570E-5	0.001795	0.002049	0.004926	0.004616
ζ_{FRP}	(15)	0.9389	0.4996	0.4165	0.196284	0.208426
σ_2^c, MPa	(14)	-2.6752	-7.6539	-8.1851	-10.2067	-9.580529
σ_1^c, MPa	(20)	2.5068	0.8598	0.8175	0.6240	0.591768
τ_{12}^c, MPa	(25)	0.002682	-0.3573	-0.6197	-1.4455	-1.099166
f_l, MPa	(26)	3.4949	391.91	396.59	433.26	438.52
f_t, MPa	(26)	3.5284	341.11	392.16	409.05	350.02
f_f, MPa	(31)	1.3370	129.26	147.55	354.72	332.35
a1ǂ	-	0.0658	6.7912	7.3729	9.5888	8.9791
a2ǂ	-	0.1684	6.7941	7.3676	9.5826	8.9887
b1ǂ	-	-0.011	-0.72469	-1.2495	-2.8992	-2.2083
b2ǂ	-	0.00536	-0.71470	-1.2395	-2.8910	2.1983
τ_{lt}, MPa	(3)	2.5547	4.2568	4.5013	5.4154	5.0861
γ_{lt}	(6)	0.000167	0.004537	0.005479	0.015443	0.025312

ǂ a1= $\rho_l f_l + \rho_{fl} f_{fl} + \rho_t f_t + \rho_{ft} f_{ft}$ b1= $\rho_l f_l + \rho_{fl} f_{fl} - \rho_t f_t - \rho_{ft} f_{ft}$

a2= $(\sigma_l + \sigma_t) - (\sigma_1^c + \sigma_2^c)$ b2= $(\sigma_l - \sigma_t) - (\sigma_1^c - \sigma_2^c)\cos 2\alpha_1 + 2\tau_{12}^c \sin 2\alpha_1$

The four points on the curves represent the first yielding point of steel, second yielding point of steel, peak point, and a typical point in the descending branch, respectively. In panel P4-040-FW the effective reinforcement ratio in longitudinal direction was less than the transversal direction, therefore, the first yield point in the shear stress versus shear strain curve is due to the yielding of the transverse steel as shown in Fig. 6a. Fig. 6b shows that the concrete compressive stress versus concrete compressive strain curve goes into the descending branch after the concrete compressive strength reaches the peak point. The concrete shear stress versus the concrete shear strain curve is shown in Fig. 6c. After the second steel yields, the slope of the curve decreases up to the peak point. The peak point of the applied shear stress (Fig. 6a) is accompanied by the peaks of concrete properties in Fig. 6b and Fig. 6c, indicating that the compressive strength (Fig. 6b) and the shear strength (Fig. 6c) of the concrete are exhausted. The transversal steel tensile stress versus biaxial and uniaxial tensile strain curves are shown in Fig. 6d and Fig. 6e, respectively. In Fig. 6e, it can be observed that the uniaxial steel strain decreases after the peak point due to stress release from the steel rebars. The strains in the transversal steel behave in an interesting way after reaching the peak point; while the uniaxial strain decreases elastically after peak point (Fig. 6e), the Poisson effect results in the significant increase of the biaxial strain along the descending branch (Fig.6d). The descending branches are predicted by incorporating the Poisson effect in the SMM-FRP shown in Fig. 6a, Fig. 6b, and Fig. 6c. While the loading history of shear stress versus shear strain curve in Fig. 6a moves from the peak point to a typical point in the descending branch, both the stresses and the strains in the

longitudinal steel increase rapidly into the strain-hardening region. Beyond the typical point, the longitudinal and transverse steel stresses decrease.

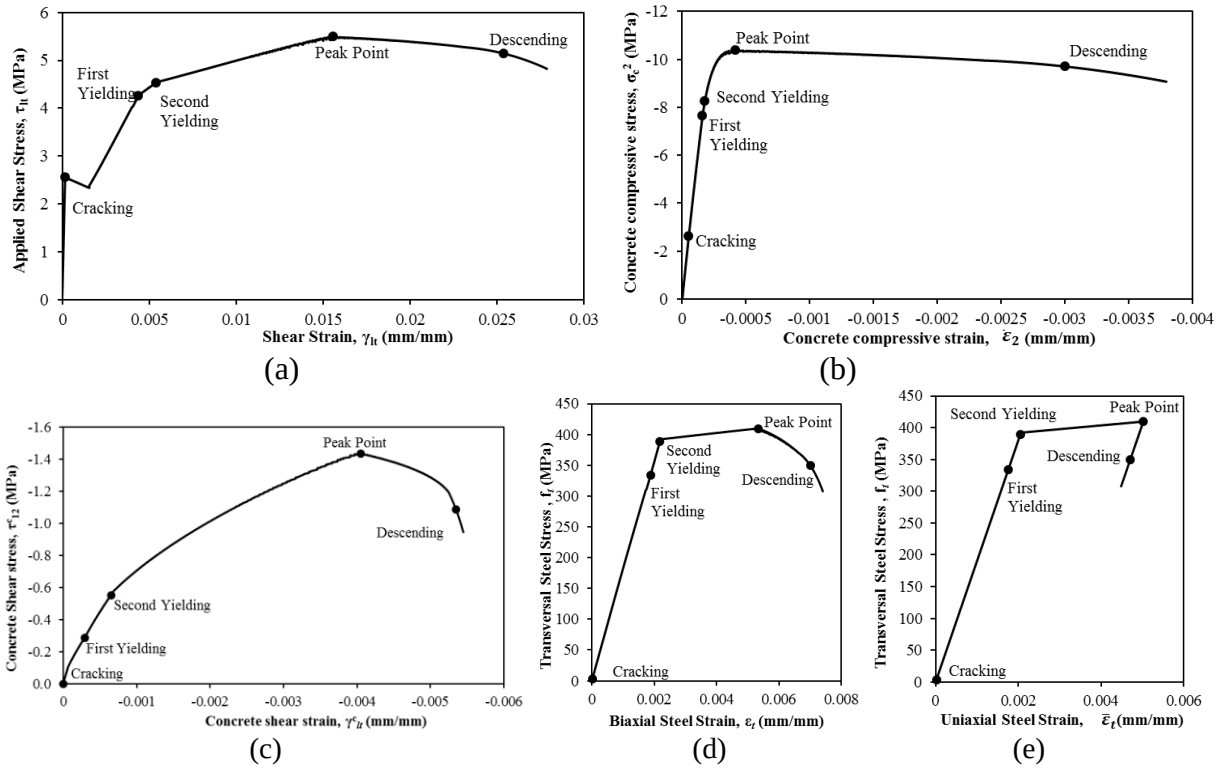

Fig. 6-(a) Applied shear stress τ_{lt} versus strain γ_{lt} curve; (b) concrete compressive stress σ_2^c versus shear strain ε_2 curve; (c) concrete shear stress τ_{12}^c versus shear strain γ_{lt}^c; (d) transversal steel stress f_t versus biaxial steel strain ε_t curve; and (e) transversal steel stress f_t versus uniaxial steel strain $\bar{\varepsilon}_t$ curve.

5. APPLICATION OF SMM-FRP TO TEST PANELS

A computer program is written according to the solution procedure in Fig. 5 to predict the shear behavior of FRP strengthened RC panels. The applied shear stresses versus shear strain relationships predicted by SMM-FRP are compared with the experimental results of 8 FRP strengthened RC panels. In Fig.7 the experimental and analytical shear stress-shear strain curves of 8 tested panels in this research are shown.

The predictions for panel series P3-FW which were reinforced with longitudinal and transversal reinforcement ratios of 0.76% and 0.43%, respectively, and strengthened with FRP fully wrapped along the transversal direction with different FRP reinforcement ratios as of $\rho_f = 0.54\%$ and $\rho_f = 0.87\%$ for panels P3-025-FW and P3-040-FW, respectively, are shown in Fig. 7. The analytical results gave conservative yield strength predictions due to the small steel reinforcement ratios in transversal direction. Also, the post crack shear strain was bigger than the experimental results which lead to a higher prediction in the post crack stiffness. This was due to neglecting the bond effect between the FRP sheets and concrete substrate which prevented the cracks from opening and was not considered in the model. The peak point in these panels where predicted to be higher than the experimental results. The conservative predictions in the yield strength of panel series P3-FW are caused by neglecting the effect of steel ratio on the softening coefficient. This effect was not taken into consideration as a variable in the softening coefficient for simplicity. When the steel reinforcement ratio decreases, the concrete struts sustain less stress and less deterioration, and the concrete contribution increases (Hsu and Zhu, 2002). Predictions of other panels which had higher steel reinforcement ratios were satisfactory.

The SMM-FRP model is a smeared model; therefore, the local failure of FRP was not captured by the model. The model predicted the shear behavior up to the failure of the strengthening system. For members which failed by concrete crushing rather than FRP rupture (P4-080-FW), the behavior especially the descending branch were modeled accurately. However, members which failed by FRP rupture (P4-040-FW),

debonding (P4-040-SB) or anchorage failure (P4-025-FA) were not modeled accurately in their descending branch.

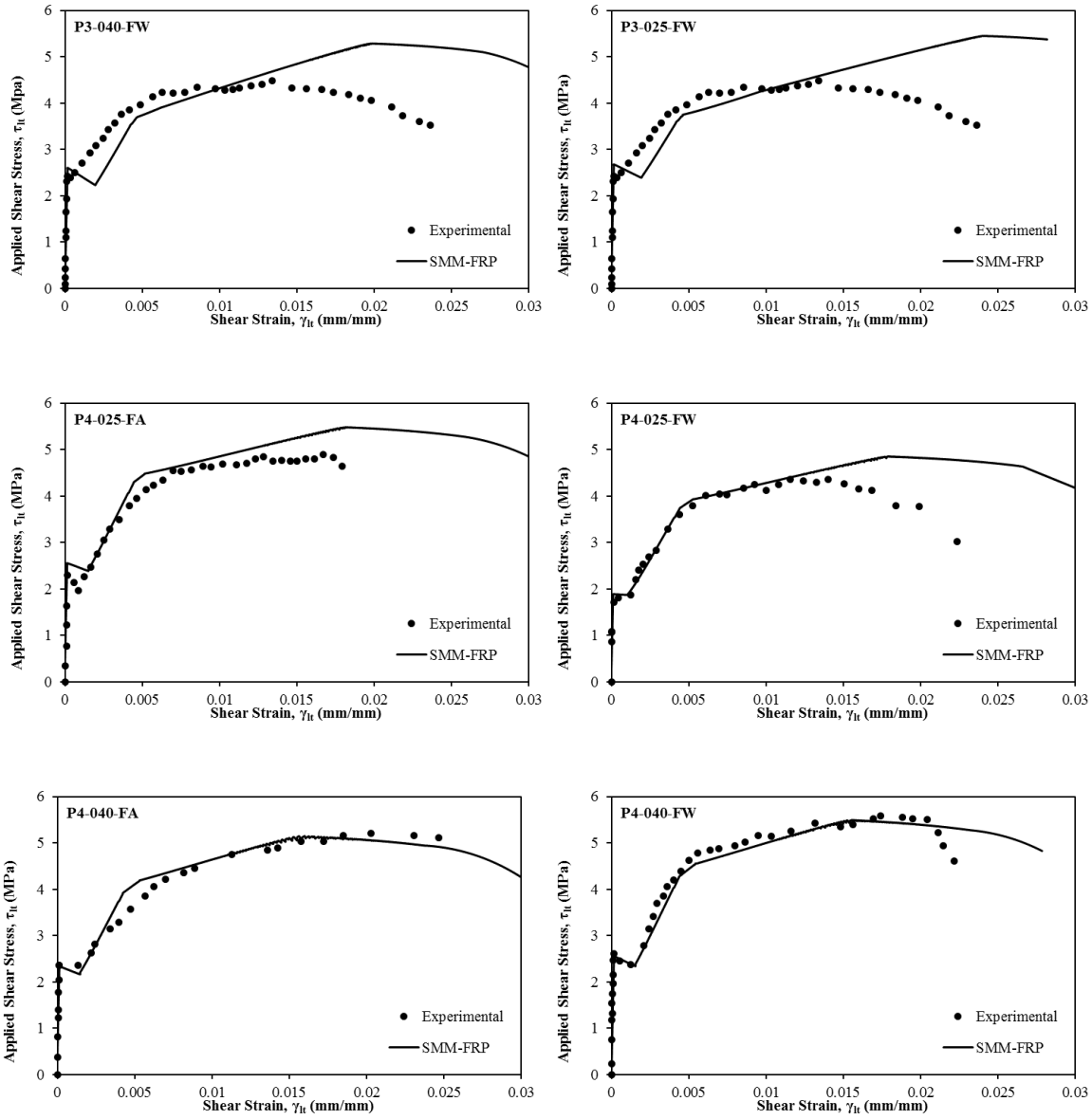

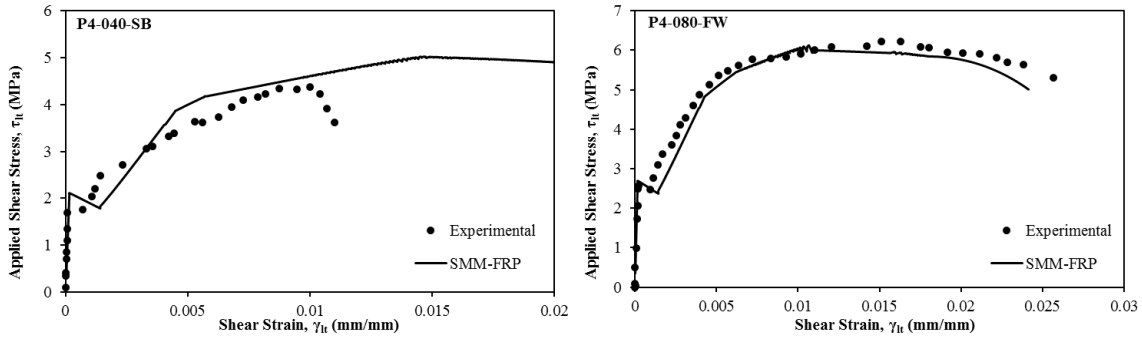

Fig. 7. Comparison of SMM-FRP with test results in terms of shear stress-shear strain curves.

6. FINITE ELEMENT FORMULATION OF SMM-FRP

Generally, there are two types of finite element modeling for cracked RC members, (1) the microscopic models and (2) the macroscopic models (Hsu and Zhang, 1997). Microscopic models are based on the stress-strain relations of plain concrete and steel. The interactions of reinforcement and steel through bond slip along the reinforcing bars and also through shear-sliding along cracked surfaces is the main focus. Due to the complicated interaction between the components which cannot be modeled either by the simple superposition of the material laws of plain concrete and steel, or by the introduction of bond and shear interface elements, the microscopic modeling is found to be inappropriate for large structures. Therefore, the macroscopic models were developed to overcome this issue. The macroscopic approach, also referred to as smeared crack concept is based on the average stress-strain relationships of concrete and steel where bond slipping and shear sliding are implicitly included (Hsu and Zhang, 1997). In this research, a nonlinear reinforced concrete finite element program is developed by implementing the SMM-FRP into the finite element framework OpenSees (McKenna and Fenves 2001). The finite

element program is validated through comparison with experimental results of panels specimens tested in this research. A uniaxial concrete model "ConcreteF01" and a steel model "SteelF01" are created based on the uniaxial constitutive relationships of concrete and steel in the SMM-FRP.

6.1. Coordinate System

In Fig. 8, three Cartesian coordinate systems defined in the reinforced concrete element, x-y, 1-2, and xi-yi, are shown. The local coordinate of the elements is represented in the x-y coordinate system. The directions of the principal stresses are defined in the 1-2 coordinate systems and have an angle θ_1 with respect to the x-y coordinate system. Furthermore, reinforcing steel bars and FRP sheets can be considered in various directions in the concrete element. Coordinate xi-yi shows the '*i*th' direction of the internal and external reinforcements with an angle θ_i with respect to the x-y coordinate system in the direction of axis x_i.

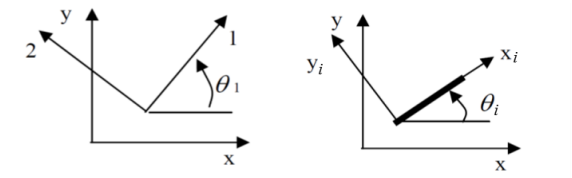

Fig. 8. Coordinate systems for FRP strengthened RC elements: (a) applied principal stresses in local coordinate (b) reinforcement component in local coordinate

The stresses and strains are transformed between coordinate systems using the transformation matrix $[T(\theta)]$ which is given as

$$[T(\theta)]=\begin{bmatrix} \cos^2\theta & \sin^2\theta & 2\sin\theta\cos\theta \\ \sin^2\theta & \cos^2\theta & -2\sin\theta\cos\theta \\ -\sin\theta\cos\theta & \sin\theta\cos\theta & \cos^2\theta-\sin^2\theta \end{bmatrix} \tag{34}$$

where θ is the angle between the two coordinate systems.

6.2. Equilibrium and Compatibility Formulations

The equilibrium equations which relate the applied stresses in the x-y coordinate (σ_x , σ_y , and τ_{xy}) to the internal concrete stresses in the principle directions (σ_1^c , σ_2^c , and τ_{12}^c), and also the stresses in the reinforcing bars (f_{si}) and FRP sheets (f_{fi}) in the directions of the reinforcements are:

$$\begin{Bmatrix} \sigma_x \\ \sigma_y \\ \tau_{xy} \end{Bmatrix} = \left[T(-\theta_1)\right] \begin{Bmatrix} \sigma_1^c \\ \sigma_2^c \\ \tau_{12}^c \end{Bmatrix} + \sum_i \left[T(-\theta_i)\right] \begin{Bmatrix} \rho_{si} f_{si} + \rho_{fi} f_{fi} \\ 0 \\ 0 \end{Bmatrix}, \text{ i=1, 2, 3,....} \quad (35)$$

where, ρ_{si} and ρ_{fi} are the rebar and FRP reinforcement ratio in the i^{th} direction, respectively; $\left[T(-\theta_1)\right]$ and $\left[T(-\theta_i)\right]$ are the transformation matrices from the 1-2 coordinate and the x_i-y_i coordinate system to the x-y coordinate system, respectively.

The compatibility equations relate the steel and FRP strains in the x_i-y_i coordinate and the concrete strain in the principle 1-2 coordinate system, expressed as:

$$\begin{Bmatrix} \varepsilon_i \\ \varepsilon_{i'} \\ \frac{1}{2}\gamma_i \end{Bmatrix} = \left[T(\theta_i - \theta_1)\right] \begin{Bmatrix} \varepsilon_1 \\ \varepsilon_2 \\ \frac{1}{2}\gamma_{12} \end{Bmatrix} \quad (36)$$

It should be noted that in Eq. (36) the reinforcement strains (ε_i) and the principle concrete strains (ε_1) are biaxial strains.

Biaxial strains are related to uniaxial strains using the Hsu/Zhu ratios (ν_{12} , ν_{21}) proposed by Hsu and Zhu (2002). The biaxial strains of concrete (ε_1 , ε_2) are

transformed to uniaxial strains of concrete ($\bar{\varepsilon}_1$, $\bar{\varepsilon}_2$) using the Hsu/Zhu ratios. Afterwards, they are transferred to the uniaxial strains of reinforcements (ε_i) as:

$$\begin{Bmatrix} \bar{\varepsilon}_1 \\ \bar{\varepsilon}_2 \\ \frac{1}{2}\gamma_{12} \end{Bmatrix} = [V] \begin{Bmatrix} \varepsilon_1 \\ \varepsilon_2 \\ \frac{1}{2}\gamma_{12} \end{Bmatrix}, \text{ where} \tag{37}$$

$$[V] = \begin{bmatrix} \frac{1}{1-\nu_{12}\nu_{21}} & \frac{\nu_{12}}{1-\nu_{12}\nu_{21}} & 0 \\ \frac{\nu_{21}}{1-\nu_{12}\nu_{21}} & \frac{1}{1-\nu_{12}\nu_{21}} & 0 \\ 0 & 0 & 1 \end{bmatrix} \text{ and} \tag{38}$$

$$\begin{Bmatrix} \bar{\varepsilon}_i \\ \bar{\varepsilon}_{i'} \\ \frac{1}{2}\gamma_i \end{Bmatrix} = [T(\theta_i - \theta_1)] \begin{Bmatrix} \bar{\varepsilon}_1 \\ \bar{\varepsilon}_2 \\ \frac{1}{2}\gamma_{12} \end{Bmatrix}. \tag{39}$$

The stresses of concrete and reinforcements in Eq. (35) are determined based on the uniaxial constitutive relationship of the materials.

The stresses and strains of an element are related with a material stiffness (constitutive) matrix. In the SMM-FRP model, the material stiffness matrix for the FRP-strengthened reinforced concrete membrane elements are defined in terms of tangent formulations. The tangent stiffness matrix $[\overline{D}]$ for an FRP-strengthened RC element is defined as:

$$[\bar{D}] = \frac{d\begin{Bmatrix}\sigma_x \\ \sigma_y \\ \tau_{xy}\end{Bmatrix}}{d\begin{Bmatrix}\varepsilon_x \\ \varepsilon_y \\ \frac{1}{2}\gamma_{xy}\end{Bmatrix}} \text{ and} \tag{40}$$

$$[\bar{D}] = [T(-\theta_1)][\bar{D}_c][V][T(\theta_1)] + \sum_i [T(-\theta_i)][\bar{D}_{ri}][T(\theta_i - \theta_1)][V][T(\theta_1)], \tag{41}$$

where $[\bar{D}_c]$ is the uniaxial tangential stiffness matrix of concrete; $[\bar{D}_{ri}]$ is the uniaxial tangential stiffness matrix of reinforcements; $[V]$ which is defined in Eq. (38) transforms the biaxial strains to uniaxial strains by using the Hsu/Zhu ratios; $[T(\theta_1)]$ is the transformation matrix from the local x-y coordinate to the 1-2 coordinate system; $[T(-\theta_1)]$ is the transformation matrix from the 1-2 coordinate to the x-y coordinate system; $[T(-\theta_i)]$ is the transformation matrix from the x_i-y_i coordinate to the x-y coordinate system; $[T(\theta_i - \theta_1)]$ is the transformation matrix from the 1-2 coordinate to the x_i-y_i coordinate system (Hsu and Mo, 2010).

The uniaxial stiffness matrix of concrete $[\bar{D}_c]$ is given as

$$[\bar{D}_c] = \begin{bmatrix} \bar{\bar{E}}_1^c & \frac{\partial \sigma_1^c}{\partial \bar{\varepsilon}_2} & 0 \\ \frac{\partial \sigma_2^c}{\partial \bar{\varepsilon}_1} & \bar{\bar{E}}_2^c & 0 \\ 0 & 0 & G_{12}^c \end{bmatrix}, \tag{42}$$

where $\bar{\bar{E}}_1^c$ and $\bar{\bar{E}}_2^c$ are the tangential uniaxial modulus of concrete in the 1 and 2 directions, respectively, which is evaluated at a certain stress/strain state. The off

diagonal terms $\frac{\partial \sigma_2^c}{\partial \bar{\varepsilon}_1}$ and $\frac{\partial \sigma_1^c}{\partial \bar{\varepsilon}_2}$ are obtained by using the uniaxial constitutive relationships and taking into account the states of the concrete stresses and uniaxial strains in the 1 and 2 directions.

The uniaxial stiffness matrix of reinforcements $[\bar{D}_{ri}]$ is evaluated as:

$$[\bar{D}_{ri}] = \begin{bmatrix} \rho_{si}\bar{\bar{E}}_{si} + \rho_{fi}\bar{\bar{E}}_{fi} & 0 & 0 \\ 0 & 0 & 0 \\ 0 & 0 & 0 \end{bmatrix}, \quad (43)$$

where $\bar{\bar{E}}_{si}$ and $\bar{\bar{E}}_{fi}$ are the uniaxial tangential modulus of rebars and FRP, respectively, determined for a particular stress/strain state. Dowel action of reinforcements is neglected since it is assumed that the FRP and Steel reinforcement only take axial stresses .

Analysis Procedure of FRP-RC Plane Stress Structures

By using the basic finite element procedure, the tangent element stiffness matrix $[K]_e$ is evaluated from the tangent material stiffness matrix $[\bar{D}]$ as:

$$[K]_e = \int_V [B]^T [\bar{D}][B] dV, \quad (44)$$

where $[B]$ which depends on the assumed displacement function is a matrix that represents the shape function of the element.

To perform nonlinear analysis of RC structures, an iterative tangent stiffness method was developed by Zhong (2005). To perform nonlinear analyses of FRP-strengthened RC structures the method was further modified. Fig. 9 describes an

iterative solution under load control using the Newton-Raphson method. The procedure for establishment of the material stiffness matrix using SMM-FRP is shown in the shaded area in Fig. 9. To obtain the material stiffness matrix, since the principal stress direction is an unknown value, a supplementary iterative loop is defined for FRP-RC plane stress elements. The method for calculating the stiffness matrix of FRP-RC plane stress elements are outlined by the outer block shown in Fig. 9.

The flow chart shown in Fig. 9, presents an analysis method for FRP-RC plane stress elements using load control. It should be noted that other integrators such as displacement control can be incorporated in the model. The incremental equilibrium equation $[K]\{\Delta u\}= \{\Delta R\}$ shown in the flow chart is for static analysis.

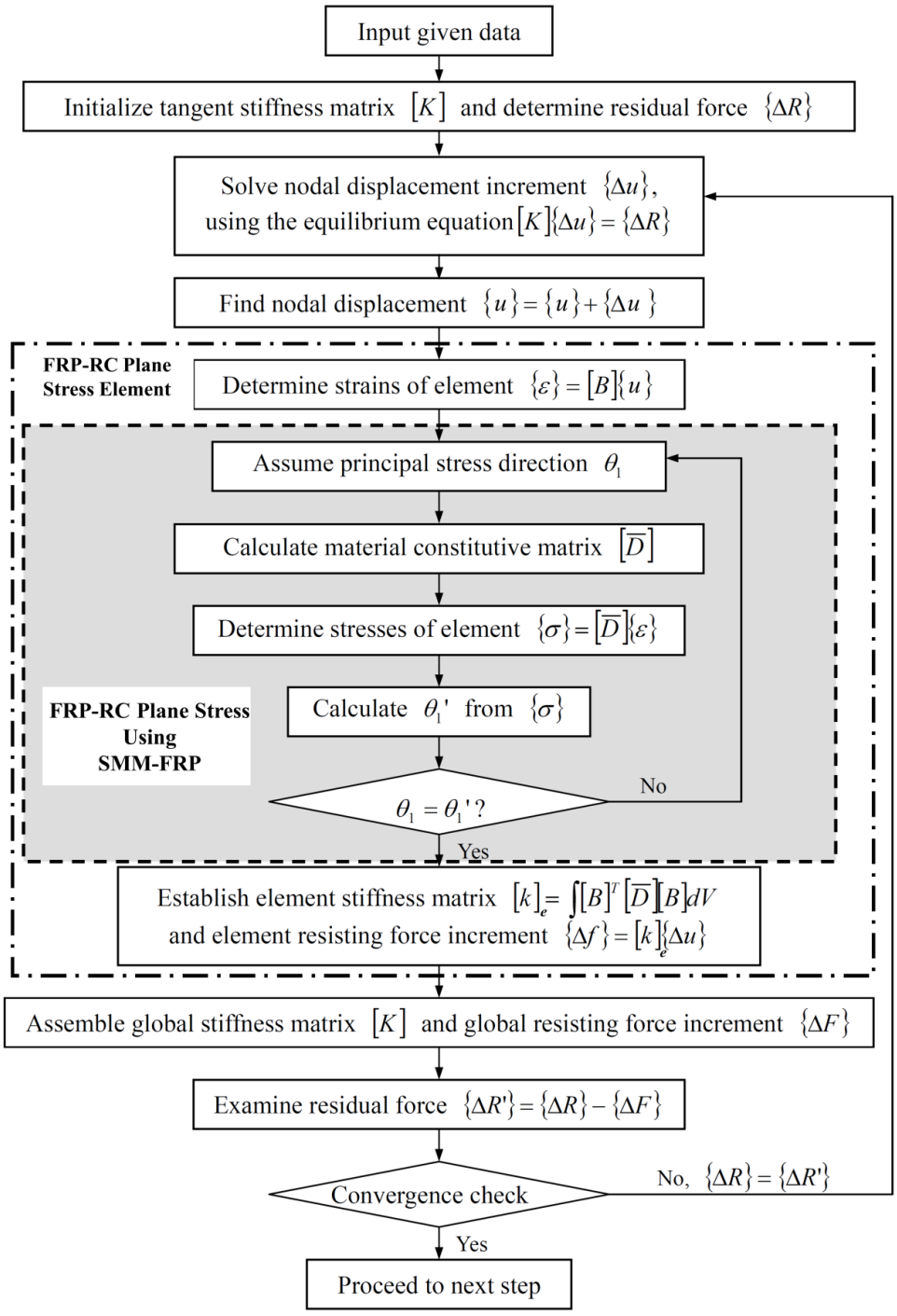

Fig. 9. Nonlinear Finite Element Analysis Algorithm (adopted from Zhong, 2005)

Convergence criterion is required to conclude if convergence has been achieved at the end of each iteration.

6.3. Implementation of the nonlinear finite element program

New material classes related to FRP-strengthened RC membrane elements are implemented into the OpenSees framework to perform analysis on FRP-strengthened RC plane stress structures Two uniaxial material models for concrete and steel in FRP-strengthened RC, namely ConcreteF01 and SteelF01 are created and implemented into OpenSees based on the ConcreteZ01 and SteelZ01 material models developed by Zhong (2005). The material model of ConcreteF01 needs five input parameters: the ultimate compressive strength f_c', the compressive strain ε_0 corresponding to f_c', FRP reinforcement ratio ρ_f, FRP Young's modulus E_f, and the parameter "*c*" of concrete in tension,. An object of SteelF01 needs the following parameters: yield stress f_y, Young's modulus E_s, concrete compressive strength f_c', and effective steel reinforcement ratio ρ_{se}.

A 2D material class named "FRPRCPlaneStress", which is a class for FRP-strengthened RC plane stress material using SMM-FRP, is created and implemented into OpenSees. In FRPRCPlaneStress, the stress vector is calculated. Furthermore, an object of FRPRCPlaneStress material needs the tags of the newly created uniaxial steel and concrete objects of SteelF01 and ConcreteF01, , the steel ratio for the steel in each direction, the directions of the steel reinforcement, concrete compressive strength, steel Young's modulus, steel yield stress, FRP reinforcement ratio, and FRP Young's modulus. Two uniaxial concrete objects are needed in defining one FRPRCPlaneStress object, which represents the concrete in the two principal stress directions.

In Fig. 10, the implementation of the FRPRCPlaneStress into OpenSees is shown. The FRPRCPlaneStress is executed with a Quadrilateral element which represents the FRP-RC plane stress elements. The FRPRCPlaneStress is related with ConcreteF0l and SteelF0l to determine the tangent stiffness matrix and to calculate element stresses.

The FRPRCPlaneStress will collect the strains of the elements in each trial, calculate the uniaxial strains of the reinforcements and concrete, then the concrete uniaxial strains and the perpendicular tensile strains are refered to the two previously defined concrete material objects. Furthermore, the concrete object will then calculate the stiffness matrix and corresponding stresses and transmit the values to the FRPRCPlaneStress object. Likewise, FRPRCPlaneStress will send the uniaxial strains of the steel to the uniaxial steel object and receive the stress and the tangent stiffness from the uniaxial steel objects.

The tangent stiffness matrix will be calculated and the stress vectors will be evaluated After receiving the uniaxial stress and stiffness of concrete, steel, and FRP materials. As shown in Fig. 9, an iterative procedure is defined to obtain the converged material stiffness matrix and stress vector for a given strain vector.

The user can define the degree of freedom of the node which controls the the solution. The displacement increment for each path of the displacement scheme can vary. To resolve numerical issues in the nonlinear analysis, the size of displacement increment is changed.

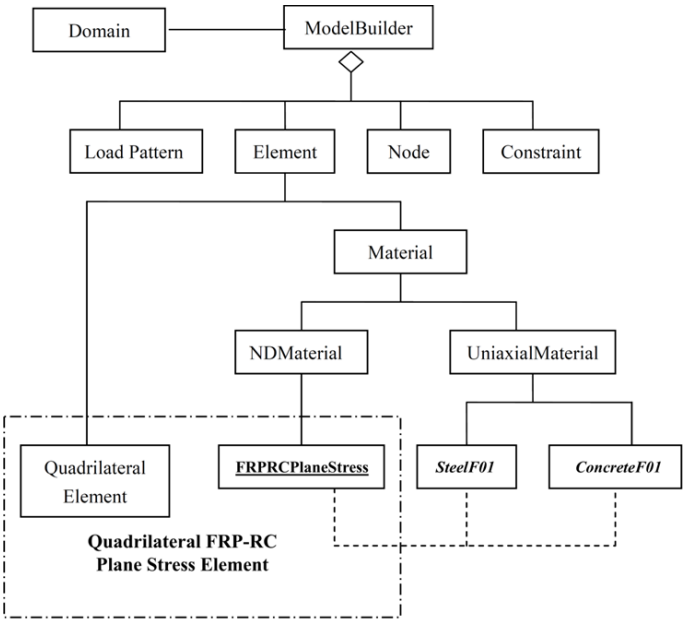

Fig. 10. Finite Element Implementation of SMM-FRP (adopted from Zhong, 2005)

The FRPRCPlaneStress material is implemented with the quadrilateral element in OpenSees, which constructs a four-node quadrilateral element object to represent the FRP-RC plane stress four node elements. The four node quadrilateral element object uses a bilinear isoparametric formulation. It should be noted that a standard isoparametric element faces many limitations such as shear locking were the displacement values could be smaller than expected. When the element is subjected to pure bending the term shear locking used to define the development of shear stresses.

6.4. Simulation of FRP-strengthened RC panels

In this section, the developed nonlinear finite element program is verified by the experimental results of FRP strengthened RC panels under monotonic shear. The reinforcement grids in all panels were set parallel to the plane of pure shear, as

shown in Fig. 11a. The panels were reinforced with different steel and FRP reinforcement ratios.

Since the material properties and stress conditions were uniform throughout all the panels, they were modeled using one 2-D FRP-RC element as shown in Fig.11b. The boundary conditions and loading scenario are defined to mimic the pure shear loading on the panel elements. In Fig. 12, the predicted panel responses are compared to the experimental.

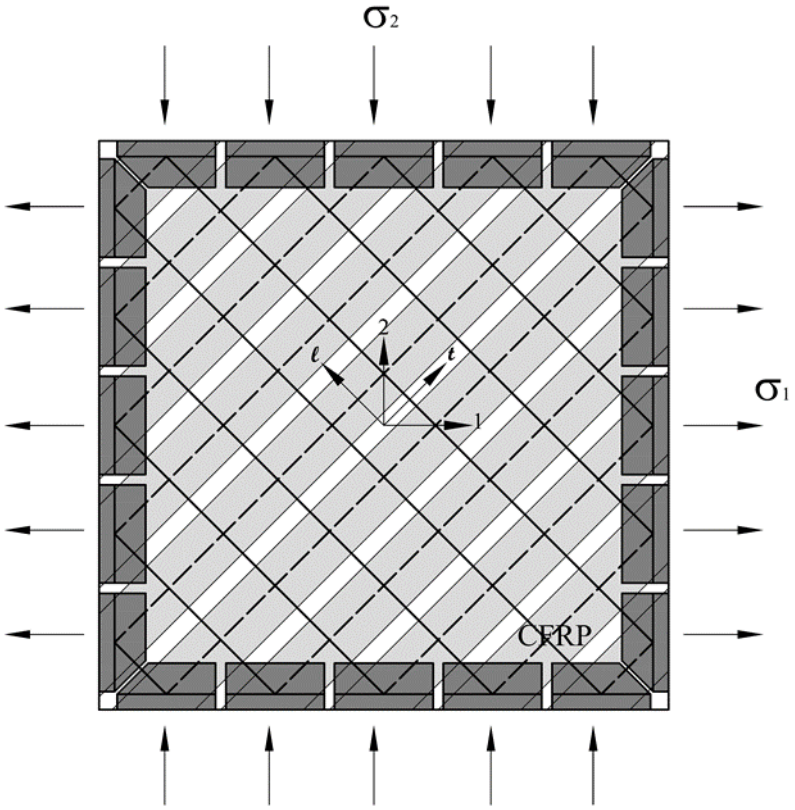

Fig.11a Reinforcement Orientation of Panel Specimens

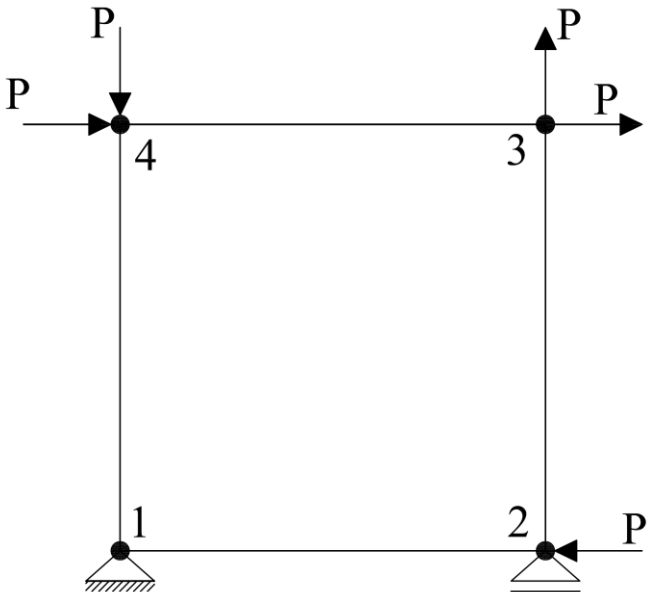

Fig. 11b Finite Element Mesh of Panel Specimens

As shown in Fig. 12, the predicted results of most of the panels for the whole loading history agree very well with the experimental results. The post cracking shear strain and the descending branches of panels REF-P3 and P3-FW series did not match well with the experimental results. This can be due to the low steel reinforcement ratios in the transversal direction in these panels. The post crack shear strain was bigger than the experimental results which lead to a higher prediction in the post crack stiffness. This was due to neglecting the bond effect between the FRP sheets and concrete substrate which prevented the cracks from opening and was not considered in the model. The predictions of panels which had higher steel reinforcement ratios were satisfactory. Panel P4-040-SB failed by debonding of FRP sheets from concrete substrate, therefore the finite element prediction was satisfactory for this panel only up to failure. The behavior of panel P4-080-FW which had the highest FRP reinforcement ratio was predicted very well in both ascending and descending branches. It can be concluded that the failure

mode has a great impact on the predictions. For panel P4-080-FW, since it failed by concrete crushing rather than FRP rupture, the behavior especially the descending branch, was modeled accurately. Other panels which failed by FRP rupture, debonding or anchorage failure were not modeled accurately in their descending branch.

The SMM-FRP is a smeared model; therefore, the local failure such as debonding of FRP and spalling of concrete was not captured by the model. Furthermore, bond-sliping and shear sliding was not considered in the model; however, they are implicitly included. The model predicted the shear behavior up to the failure of the strengthening system. Moreover, the proposed SMM-FRP model is a two-dimensional model under plane stress conditions. These could be considered as the limitations of the developed finite element model.

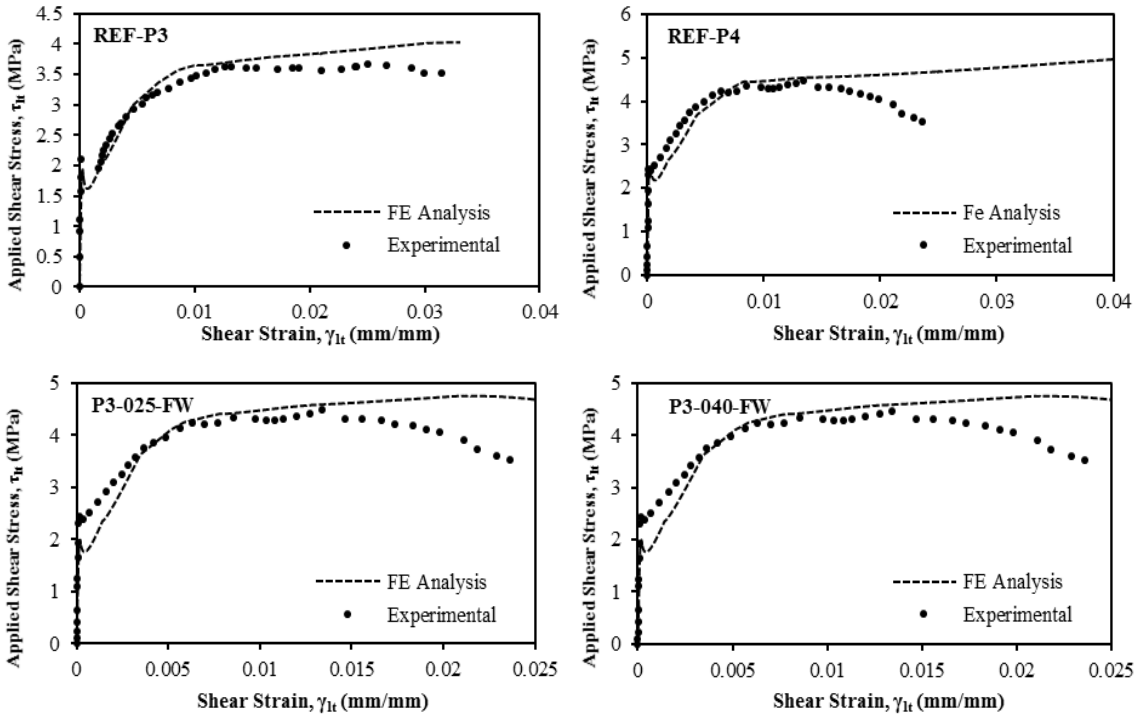

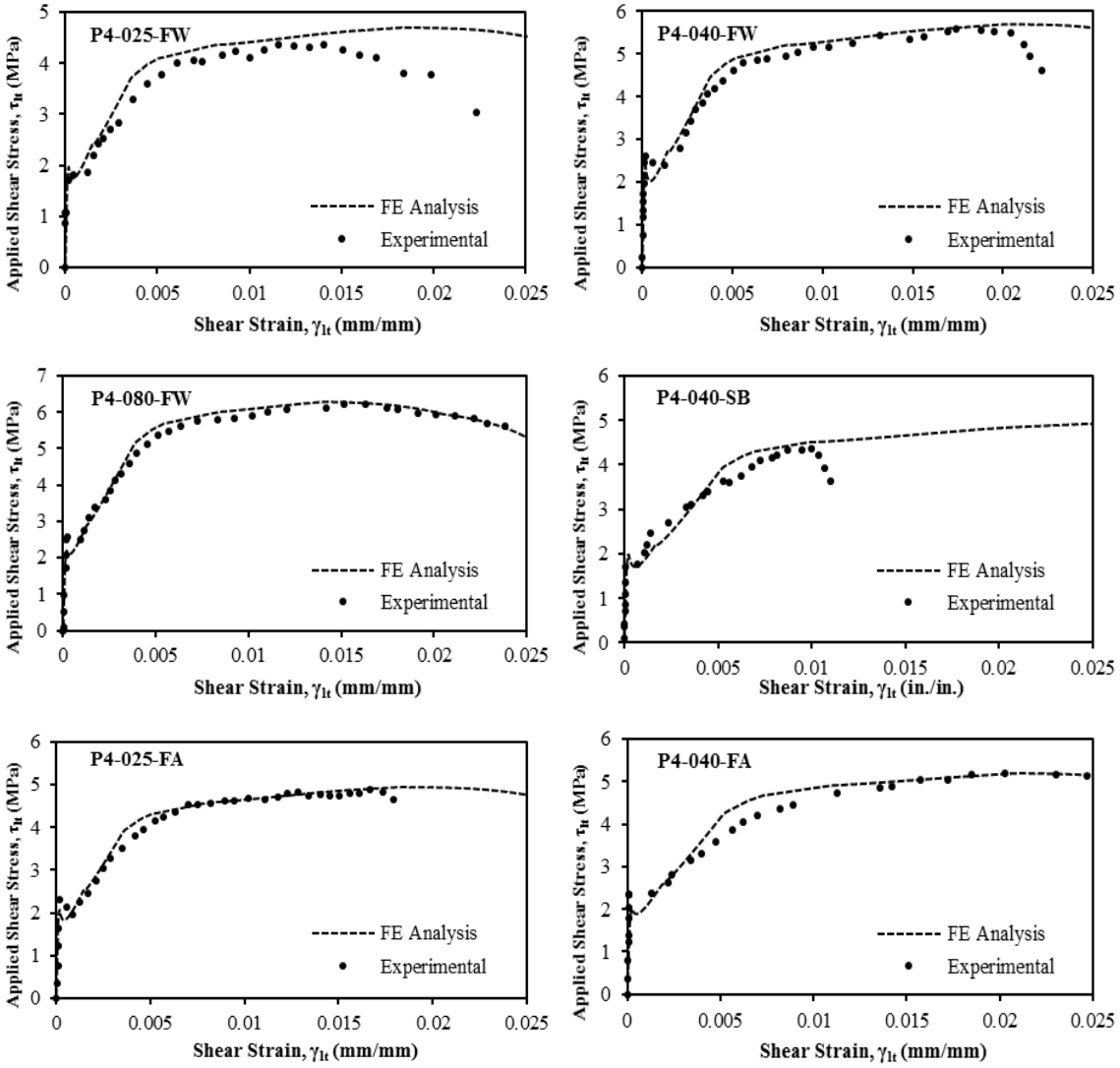

Fig. 12 Comparison of Experimental and Finite Element Analysis of Panels

The comparison of shear stress and shear strain curves between the experimental panel tests and two different SMM finite element analyses of panels P4-040-FW and P4-040-FW are shown in Fig. 13. One is the SMM with the original constitutive laws of concrete and steel in tension for RC members with just the addition of the FRP reinforcements in the equilibrium equations. The other one is the SMM-FRP which includes all the new interacting material models for concrete, steel, and FRP. It can be seen that the original model underestimated the tension stiffening effect of concrete, while the SMM-FRP model with modified constitutive laws shows a much

better prediction. The new softening equations and also the new Poisson's ratio resulted in a better prediction of the behavior, especially in the descending portion of the curves.

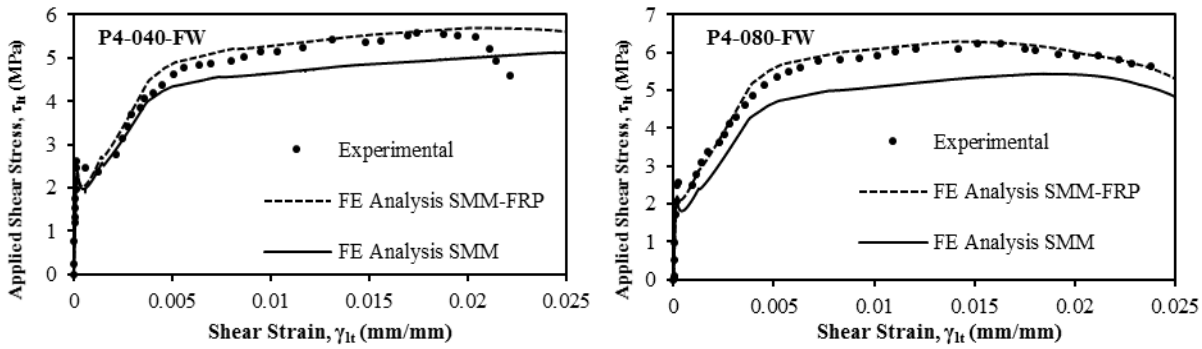

a) Panel P4-040-FW b) Panel P4-080-FW

Fig. 13 Comparison of SMM and SMM-FRP Finite Element models of Panels

CONCLUSIONS

In this study, an analytical model (SMM-FRP) is proposed to predict the full shear behavior of FRP strengthened RC members. The SMM-FRP is an extension of the SMM. By using an iterative solution algorithm, the equilibrium equations, compatibility equations and the new constitutive relationships of materials deduced in this study are combined to calculate the unknown variables. The main conclusions are as follows:

1. The comparison between the theoretical values calculated by SMM-FRP and the experimental results of 10 panels indicates a good prediction for the overall shear behavior of the FRP strengthened RC members, including pre-cracking and post-cracking behavior.

2. More reasonable compressive and tensile constitutive relationships of FRP strengthened RC members subjected to shear loading that take into account the effect of externally bonded FRP sheets are utilized in the proposed model.

3. It was observed that the original SMM model underestimated the tension stiffening effect of concrete for FRP strengthened RC members, while the SMM-FRP model with modified constitutive laws and the new softening equations and Poisson's ratios resulted in a better prediction of the behavior, especially in the descending portion of the shear stress-strain relationship.

ACKNOWLEDGMENTS

The authors would like to acknowledge the financial support provided by the National Science Foundation (NSF), award number 1100930. Steel reinforcements and FRP materials were a donation from Gerdau Ameristeel Co. and FYFE. Co, respectively. Their support is greatly acknowledged.

Nomenclature

The following symbols are used in this paper:

B	factor for calculating apparent yielding stress
c	coefficient for tension stiffening
E_c	modulus of elasticity of concrete
$\overline{\overline{E}}_1^c$	tangent uniaxial modulus of concrete in 1-direction
$\overline{\overline{E}}_2^c$	tangent uniaxial modulus of concrete in 2-direction
E_f	tensile modulus of elasticity of FRP
$\overline{\overline{E}}_{fi}$	tangent uniaxial modulus of elasticity of FRP in i^{th} direction
E_s	modulus of elasticity of steel
$f_c^{'}$	specified compressive strength of concrete
f_{cr}	cracking tensile strength of concrete

f_{fe}	effective stress in FRP
f_{fi}	stress FRP sheets in the i^{th} direction
f_{fl}	smeared (average) stress in FRP in *l*-direction
f_{ft}	smeared (average) stress in FRP in *t*-direction
f_l	smeared (average) stress in embedded mild steel rebars in *l*-direction
f_{ly}	yield stress of mild steel rebars in *l*-direction
f_s	smeared (average) stress in embedded mild steel rebars
f_{si}	stress of steel rebars in the i^{th} direction
f_t	smeared (average) stress in embedded mild steel rebars in *t*-direction
f_{ty}	specified yield strength of steel rebars reinforcement in *t*-direction
f_u	specified ultimate tensile strength of steel reinforcement
$f_{u,FRP}$	ultimate tensile strength of FRP sheet
f_y	specified yield strength for reinforcement
$f_y^{'}$	apparent yield stress of steel rebar
G_{12}^{c}	shear modulus of concrete in 1-2 coordinate
k	factor considering the wrapping scheme effect in crack spacing
k_1	bond coefficient
k_2	loading coefficient
$K_{f/s}$	factor for FRP/steel stiffness ratio
K_w	factor for wrapping scheme
l	direction of longitudinal steel bars
n	number of layers of tensile reinforcement

$n_{f/s}$	ratio of Young's Modulus between FRP and steel
t	direction of transverse steel bars
t_i	local coordinate of steel layer in i^{th} direction where t_i is the direction perpendicular to the steel layer
$\boldsymbol{t}_s$	direction of transverse steel bars
x	local coordinate of RC/FRPRC element
y	local coordinate of RC/FRPRC element
α	angle of transverse reinforcement relative to the longitudinal axis
α_F	orientation angle of the fibers with respect to longitudinal axis
β	deviation angle
$\Delta\varepsilon_1$	change of strain in principal 1-direction
$\Delta\varepsilon_2$	change of strain in principal 2-direction
ε_0	concrete cylinder strain corresponding to peak cylinder strength $f_c^{'}$
ε_1	smeared (average) tensile strain in principal 1-direction
ε_2	smeared (average) tensile strain in principal 1-direction
ε_{cr}	cracking tensile strain of concrete
ε_f	strain in FRP
ε_{fe}	effective strain in FRP
ε_{fu}	design rupture of FRP reinforcement
ε_l	smeared (average) strain of steel bars in *l*-direction
ε_{sf}	smeared (average) strain of steel rebars that yield first
ε_t	smeared (average) strain of steel bars in *t*-direction

$\varepsilon_y^{'}$	strain corresponding to apparent yield strength of steel reinforcement in SMM
$\bar{\varepsilon}_1$	smeared (average) strain in 1-direction when panel is subjected to uniaxial loading
$\bar{\varepsilon}_2$	smeared (average) strain in 2-direction when panel is subjected to uniaxial loading
$\bar{\varepsilon}_l$	smeared (average) strain of steel rebar in *l*-direction when Hsu/Zhu ratios are assumed to be zero
$\bar{\varepsilon}_s$	strain in mild steel, $\bar{\varepsilon}_s$ becomes $\bar{\varepsilon}_l$ and $\bar{\varepsilon}_t$, when applied to the longitudinal and transverse steel, respectively.
$\bar{\varepsilon}_t$	smeared (average) strain of steel rebar in *t*-direction when Hsu/Zhu ratios are assumed to be zero
γ_{12}	smeared (average) shear strain in 1-2 coordinate
γ_{12}^c	smeared (average) concrete shear strain in 1-2 coordinate
γ_{120}	smeared (average) shear strain in 1-2 coordinate at maximum shear stress
γ_{lt}	smeared (average) shear strain in *l*-*t* coordinate
ν_{12}	Hsu/Zhu ratio (ratio of resulting tensile strain to source compressive strain)
ν_{21}	Hsu/Zhu ratio (ratio of resulting compressive strain to source tensile strain)
θ	angle of diagonal compression
ρ_f	FRP reinforcement ratio
ρ_{fl}	FRP reinforcement ratio in *l*-direction
ρ_{ft}	FRP reinforcement ratio in *t*-direction
ρ_{se}	equivalent reinforcement ratio
ρ_l	steel reinforcement ratio in *l*-direction

ρ_s	ratio of steel reinforcement
ρ_t	steel reinforcement ratio in *t*-direction
σ_1	smeared (average) tensile stress in principal 1-direction
σ_1^c	smeared (average) tensile stress of concrete in principal 1-direction
σ_2	smeared (average) compressive stress in principal 2-direction
σ_2^c	smeared (average) compressive stress of concrete in principal 2-direction
σ_f	smeared (average) tensile stress in FRP sheet
σ_l	smeared (average) tensile stress in *l*-direction
σ_l^c	stress resisted by concrete in *l*-direction
σ_t	smeared (average) tensile stress in *t*-direction
σ_t^c	stress resisted by concrete in *t*-direction
τ_{lt}	smeared (average) applied shear stress in *l*-*t* coordinate
τ_{12}^c	smeared (average) concrete contribution to shear stress in 1-2 coordinate
τ_{lt}^c	smeared (average) concrete contribution to shear stress in *l*-*t* coordinate
ζ_{FRP}	softening coefficient considering FRP sheet
$[B]$	matrix representing the shape function of the element
$[\overline{D}]$	tangent material stiffness matrix
$[\overline{D}_c]$	uniaxial tangential stiffness matrix of concrete
$[\overline{D}_{ri}]$	uniaxial tangential stiffness matrix of reinforcements
$[K]_e$	element stiffness matrix
$[K]$	global stiffness matrix
$[T(-\theta_i)]$	transformation matrix

$[V]$ Hsu/Zhu matrix

$\{\Delta f\}$ element resisting force increment vector

$\{\Delta F\}$ global resisting force increment vector

$\{\Delta R\}, \{\Delta R'\}$ residual force vector

$\{u\}$ nodal displacement vector

$\{\Delta u\}$ nodal displacement increment vector

$\{\varepsilon\}$ applied strain vector of the plane stress element

$\{\sigma\}$ applied stress vector of the plane stress element

REFERENCES

Belarbi, A. (1991). Stress-strain relationships of reinforced concrete in biaxial tension-compression (Doctoral dissertation). Department of Civil and Environmental Engineering, University of Houston, Houston, TX.

Belarbi, A., & Hsu, T. T. C. (1994). Constitutive laws of concrete in tension and reinforcing bars stiffened by concrete. ACI Structural Journal, 91(4), 465-474.

Belarbi, A., & Hsu, T. T. C. (1995). Constitutive laws of softened concrete in biaxial tension compression. ACI Structural Journal, 92(5), 562-573.

Bousselham A., and Chaallal O. (2008). Mechanisms of shear resistance of concrete beams strengthened in shear with externally bonded FRP. *Journal of Composite for Constructions*, *12*(5), 499-512.

Chen G. M., Teng J. G., & Chen J. F. (2010). Interaction between steel stirrups and shear-strengthening FRP strips in RC Beams. Journal of Composite for Constructions, 14(5), 498-509.

Hsu, T. T. C. & Mo. Y. L. (2010). Unified theory of concrete structures. West Sussex, UK: John Wiley and Sons Ltd.

Hsu, T. T. C., & Zhang, L. X. (1997). Nonlinear analysis of membrane elements by Fixed-Angle Softened-Truss Model. Structural Journal of the American Concrete Institute, 94(5), 483-492.

Hsu, T.T.C., & Zhu, R. R. H. (2002). Softened membrane model for reinforced concrete elements in shear. *Structural Journal of the American Concrete Institute*, *99*(4), 460-469.

Hsu, T.T.C., & Zhu, R. R. H. (2002). Softened membrane model for reinforced concrete elements in shear. Structural Journal of the American Concrete Institute, 99(4), 460-469.

Hsu, T.T.C., Zhang, L.X. & Gomez, T. (1995). A servo-control system for universal panel tester. Journal of Testing and Evaluations (ASTM), 23 (6). 424-430.

McKenna, F. & Fenves, G. L. (2002). The OpenSees command language primer. University of California, Berkeley, CA.

Pang, X. B., & Hsu, T. T. C. (1995). Behavior of reinforced concrete membrane elements in

shear. ACI Structural Journal, 92(6), 665-679.
Pang, X. B., & Hsu, T. T. C. (1996). Fixed-Angle Softened-Truss Model for reinforced concrete. ACI Structural Journal, 93(2), 197-207.
Yang G, Zomorodian M, Belarbi A, Acun B (2014). Tension stiffening of reinforced concrete shear elements strengthened with externally bonded FRP sheets. In: 37th IABSE Symposium Madrid. Madrid (Spain). p. 145–52.
Yang G, Zomorodian M, Belarbi A (2017). "Material Laws of FRP-Strengthened RC Element in Biaxial Tension–Compression." J. Compos. Constr., 10.1061/(ASCE)CC.1943-5614. 0000804.
Yang G, Zomorodian M, Belarbi A, and Ayoub A. (2015). "Uniaxial Tensile Stress-Strain Relationships of RC Elements Strengthened with FRP Sheets." J. Compos. Constr., 10.1061/(ASCE)CC.1943-5614.0000639, 04015075.
Zhong, J. (2005). Model-based simulation of reinforced concrete plane stress structures (Doctoral dissertation). Department of Civil and Environmental Engineering, University of Houston, Houston, TX.
Zhu, R. H., Hsu, T. T. C., & Lee, J. Y. (2001). Rational shear modulus for smeared crack analysis of reinforced concrete. Structural Journal of the American Concrete Institute, 98(4), 443-450.
Zhu, R. R. H. (2000). Softened-membrane model of cracked reinforced concrete considering Poisson effect (Doctoral dissertation). Department of Civil and Environmental Engineering, University of Houston, Houston, Texas.
Zomorodian, M., Yang, G., Belarbi, A., and Ayoub, A. S. (2016). "Cracking behavior and crack width predictions of FRP-strengthened RC members under tension." Eng. Struct., 125, 313-324.
Zomorodian, M. (2015). Behavior of FRP Strengthened Concrete Panel Elements Subjected to Pure Shear (Doctoral dissertation). Department of Civil and Environmental Engineering, University of Houston, Houston, Texas.